

Collision strengths and transition probabilities for Co III forbidden lines

P.J. Storey¹, Taha Sochi^{1*}

¹*Department of Physics and Astronomy, University College London, Gower Street, London WC1E 6BT, UK*

Accepted 2016 March 31. Received 2016 March 23; in original form 2016 February 01.

ABSTRACT

In this paper we compute the collision strengths and their thermally-averaged Maxwellian values for electron transitions between the fifteen lowest levels of doubly-ionised cobalt, Co^{2+} , which give rise to forbidden emission lines in the visible and infrared region of spectrum. The calculations also include transition probabilities and predicted relative line emissivities. The data are particularly useful for analysing the thermodynamic conditions of supernova ejecta.

Key words: atomic data – atomic processes – radiation mechanisms: non-thermal – supernovae: general – infrared: general.

1 INTRODUCTION

Cobalt is an iron-group element but is the least abundant of this group with a solar abundance of about 300 times less than Fe. However, in supernova (SN) ejecta it is much more abundant. For example, in SN 1987A the ratio of Co to Fe, 255 days after outburst, is approximately 0.2 by number (Varani *et al* 1990). The spectral lines of Co are therefore valuable investigative tools in analysing the chemical and thermodynamic conditions of supernovae where these emissions are mostly found. These lines are also useful in investigating the evolutionary history and chemical development by nucleosynthesis and decay processes within the SN explosions (Colgate & McKee 1969; Axelrod 1980; Kuchner *et al* 1994; Bowers *et al* 1997; Liu *et al* 1997; Churazov *et al* 2014; Childress *et al* 2015). The lines of Cobalt have also been observed in the spectral emissions of astronomical objects with more normal Co abundances such as planetary nebulae (Baluteau *et al* 1995; Zhang *et al* 2005; Pottasch & Surendiranath 2005; Wang & Liu 2007; Fang & Liu 2011).

Little computational and experimental work has been done previously to generate essential atomic data for Co III and none of the previous work deals with excitation of Co^{2+} levels by electron impact. Hansen *et al* (1984) calculated magnetic dipole and electric quadrupole transition probabilities in the $3d^7$ ground configuration of Co III using parametric fitting to the observed energy levels and Hartree-Fock values for the electric quadrupole moments. In their investigation of the forbidden transition probabilities relevant to

the analysis of infrared lines from SN 1987A, Nussbaumer & Storey (1988) provided a few transition probabilities for low levels of Co III assuming LS -coupling. Tankosić *et al* (2003) calculated Stark broadening data for a number of Co III spectral lines as a function of temperature by using a semi-empirical approach. Experimental investigations have also been conducted by Sugar & Corliss (1981, 1985) where atomic data related to Co III transitions, mainly energy levels of Co^{2+} , have been collected. Very recently, Fivet *et al* (2016) calculated radiative probabilities of Co III forbidden transitions between low-lying levels of doubly ionised cobalt as part of a larger investigation of the radiative rates in doubly ionised iron-peak elements.

We have recently reported a calculation of atomic parameters for energetically low-lying levels of Co^+ (Storey *et al* 2016). In this paper we present a similar calculation of atomic parameters related to forbidden transitions in Co^{2+} , which includes lines ranging from the visible to the three mid-infrared lines which arise from transitions within the ground term at 11.88, 16.39 and 24.06 μm . The paper primarily addresses a shortage in collisional atomic data which forced some researchers (Dessart *et al* 2014; Childress *et al* 2015) to adopt collision strengths generated for Ni IV (Sunderland *et al* 2002) as a substitute for corresponding data of Co III justifying this by the fact that the two ions possess similar electronic and term structures. Our principal result is collision strengths and their thermally-averaged Maxwellian values for electron excitation and de-excitation between the fifteen lowest levels of Co^{2+} . The study also includes the most important radiative transition probabilities for the same levels. The main tools used in generating

* E-mail: t.sochi@ucl.ac.uk

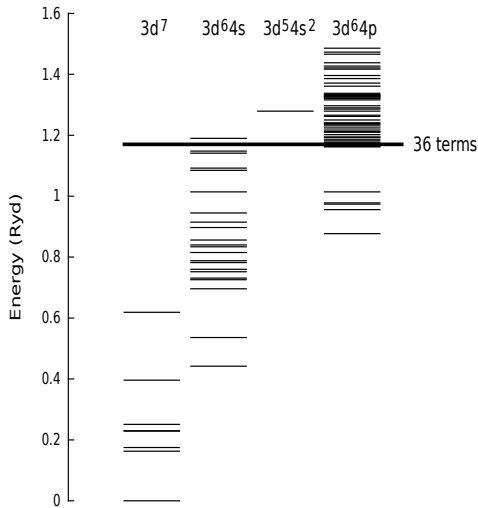


Figure 1. Schematic term energy diagram of Co III. The heavy solid line shows the extent of the close-coupled target states.

these data are the R-matrix atomic scattering code (Berrington *et al* 1974, 1987; Hummer *et al* 1993; Berrington *et al* 1995)¹ and the general purpose AUTOSTRUCTURE code (Eissner *et al* 1974; Nussbaumer & Storey 1978; Badnell 2011)². The scattering calculations were performed using a 10-configuration atomic target within a Breit-Pauli intermediate coupling approximation, as will be detailed in Section 2.

The paper is structured as follow. In Section 2 the Co^{2+} model is presented and the resulting transition probabilities are given, whereas in Section 3 the Breit-Pauli R-matrix $\text{Co}^{2+} + e$ scattering calculation is described. Results and general analysis related to the diagnostic potentials of some transitions appear in Section 4, and section 5 concludes the paper.

2 Co^{2+} ATOMIC STRUCTURE

2.1 The scattering target

A schematic diagram of the term structure of Co III up to 1.5 Rydberg is shown in Figure 1. The extent of our target is shown by the heavy solid line in that figure and includes 36 terms and 109 levels. The lowest 21 terms of this ion are of even parity from the configurations $3d^7$ and $3d^6 4s$. Transitions from higher terms give rise to lines that should be weaker at the typical temperatures of supernova ejecta and hence they will be ignored. The odd-parity terms of the $3d^6 4p$ configuration are expected to give rise to resonances that affect the collision strengths for excitation of the low-lying even-parity levels and hence they are included in the target for the scattering calculations.

A set of ten electron configurations, listed in Table 1,

Table 1. The ten target configuration basis where the core electronic structure ($[\text{Ar}]$) is suppressed. The bar indicates a correlation orbital.

$3d^7$
$3d^6 \ 4s, \ 4p, \ \bar{4}d$
$3d^5 \ 4s^2, \ 4p^2, \ \bar{4}d^2, \ 4s4p, \ 4s\bar{4}d, \ 4p\bar{4}d$

Table 2. Potential scaling parameters. The bar over the principal quantum number signifies a correlation orbital.

1s	1.42912				
2s	1.13799	2p	1.08143		
3s	1.06915	3p	1.05203	3d	1.04962
4s	1.03440	4p	1.02977	$\bar{4}d$	1.51187

were used to expand the target states. The target wavefunctions were generated with the AUTOSTRUCTURE program, (Eissner *et al* 1974; Nussbaumer & Storey 1978; Badnell 2011) using radial functions computed within scaled Thomas-Fermi-Dirac statistical model potentials. The scaling parameters were determined by minimising the sum of the energies of all the target terms, computed in LS -coupling, i.e. by neglecting all relativistic effects. The resulting scaling parameters, λ_{nl} , are given in Table 2.

In Table 3 a comparison is made between the term energies calculated using our scattering target with experimental values for the 36 terms of the target. The term energies are computed with the inclusion of one-body relativistic effects, the Darwin and mass terms, and the spin-orbit interaction. This is the type of approximation that we applied for the scattering calculations in the R-matrix code. In Table 4 the calculated energies of the 15 lowest levels are compared with the corresponding experimental values. The table also shows the values obtained by including the two-body fine structure interactions as described by Eissner *et al* (1974). The calculated fine-structure splittings of these levels are improved by this inclusion. For the total fine-structure splitting of the six terms, the average absolute difference from experiment drops from 7.3% to 4.6%.

A widely-accepted measure for the quality of the scattering calculations is the degree of agreement between weighted oscillator strengths, gf , calculated in the velocity and length formulations, where good agreement is regarded as necessary but not sufficient condition for the quality of the target wavefunctions. Table 5 provides this comparison where it shows an average difference in the absolute values of gf of about 5.8% between the two formulations, which in our view is acceptable for an open d-shell atomic system.

2.2 Transition probabilities

The forbidden transition probabilities between the even parity low-lying terms are calculated using the afore-described target wavefunctions, with empirical adjustments to the computed energies to ensure more reliable calculation of the fine-structure interactions and accurate energy factors connecting the *ab initio* calculated line strengths to the transition probabilities. The results for the lowest 15 levels are given in Table 10 where the values represent the sum of

¹ See Badnell: R-matrix write-up on WWW. URL: amdpp.phys.strath.ac.uk/UK_RmaX/codes/.

² See Badnell: AUTOSTRUCTURE write-up on WWW. URL: amdpp.phys.strath.ac.uk/autos/.

Table 3. Energies of the 36 target terms in cm^{-1} , ordered according to the experimental energy. The calculated values include only the spin-orbit contribution to the fine-structure energies. Core electronic structure ([Ar]) is suppressed from all configurations.

Config.	Term	Term Energy		
		Exp. [†]	Calc.	
3d ⁷	a ⁴ F	0	0	
	a ⁴ P	14561	17891	
	a ² G	16510	19120	
	a ² P	19618	25103	
	a ² H	22227	25205	
	a ² D	22712	27507	
	a ² F	36372	43416	
	3d ⁶ 4s	a ⁶ D	46230	48501
		a ⁴ D	55448	58817
		b ⁴ P	70965	79599
a ⁴ H		71096	76483	
b ⁴ F		72717	80163	
a ⁴ G		76219	83370	
b ² P		76521	85780	
b ² H		76690	82428	
b ² F		78323	86408	
b ² G		81793	89400	
3d ⁶ 4p	b ⁴ D	83031	92162	
	a ² I	84676	91484	
	c ² G	85485	93867	
	b ² D	90897	98436	
	z ⁶ D ^o	97807	97268	
	3d ⁶ 4s	² S		100359
	3d ⁶ 4p	z ⁶ F ^o	102620	102460
	3d ⁶ 4s	² D		103690
	3d ⁶ 4p	z ⁶ P ^o	104861	104906
	3d ⁶ 4s	z ⁴ D ^o	106074	106802
z ⁴ F ^o		106676	107272	
z ⁴ P ^o		109902	111225	
² F			111250	
⁴ F			119049	
⁴ P			119600	
² F			125226	
² P			125937	
3d ⁶ 4p		z ⁴ S ^o	122305	129103
z ⁴ G ^o		124219	127494	

[†]Experimental energies are from NIST (www.nist.gov).

the electric quadrupole and magnetic dipole contributions for each transition. This table includes only those probabilities from a given upper level which exceed 1% of the total probability from that level.

The infrared lines of principal interest here arise from transitions between the levels of the ground ⁴F term and are predominantly of magnetic dipole type. There is therefore a stepwise decay through the levels and only three relevant transition probabilities, for $a^4F_{3/2} - a^4F_{5/2}$, $a^4F_{5/2} - a^4F_{7/2}$ and $a^4F_{7/2} - a^4F_{9/2}$. We are aware of only two previous calculations of transition probabilities for Co III, one by Hansen *et al* (1984) and one by Nussbaumer & Storey (1988), as well as one contemporary calculation by Fivet *et al* (2016). Nussbaumer & Storey (1988) only give values for these three probabilities and these differ by less than 1% from our values. Hansen *et al* (1984) give more extensive results which we compare with the present values in Table 10. We find excellent agreement with Hansen *et al* (1984) for the magnetic dipole transitions between the levels of individual terms with differences of a few percent or less. There

Table 4. Energies in cm^{-1} of the 15 lowest levels of Co²⁺, ordered according to the experimental energy, where the configuration of all levels is [Ar] 3d⁷.

Index	Level	Exp. ¹	Calc. ²	Calc. ³
1	a ⁴ F _{9/2}	0.	0.	0.
2	a ⁴ F _{7/2}	841	810	824
3	a ⁴ F _{5/2}	1451	1408	1428
4	a ⁴ F _{3/2}	1867	1819	1842
5	a ⁴ P _{5/2}	15202	18481	18502
6	a ⁴ P _{3/2}	15428	18770	18785
7	a ⁴ P _{1/2}	15811	19125	19118
8	a ² G _{9/2}	16978	19565	19581
9	a ² G _{7/2}	17766	20348	20357
10	a ² P _{3/2}	20195	25601	25633
11	a ² P _{1/2}	20919	26486	26474
12	a ² H _{11/2}	22720	25690	25687
13	a ² D _{5/2}	23059	27795	27804
14	a ² H _{9/2}	23434	26367	26379
15	a ² D _{3/2}	24237	29058	29033

¹ Sugar & Corliss 1985.

² Calculated with only spin-orbit interaction.

³ As 2 plus two-body fine-structure interactions for the first 4 configurations of Table 1.

Table 5. Weighted *LS* oscillator strengths, *gf*, in the length and velocity formulations from the two energetically lowest terms of the 3d⁷ and 3d⁶4s configurations.

Transition				<i>gf_L</i>	<i>gf_V</i>
3d ⁷	⁴ F	–	3d ⁶ 4p ⁴ D ^o	2.34	2.48
		–	⁴ F ^o	1.16	1.21
		–	³ G ^o	2.38	2.30
3d ⁶ 4s	⁶ D	–	3d ⁶ 4p ⁶ D ^o	9.45	9.75
		–	⁶ F ^o	13.7	13.5
		–	⁶ P ^o	5.77	4.83

are larger differences for the electric quadrupole transition probabilities between terms. For example the probabilities for the principal transitions between the ⁴F and ⁴P terms, the 5-1, 5-2 and 5-3 probabilities, are all larger, by on average 13%, in our calculation than in Hansen *et al* (1984). The fact that all three transitions differ by approximately the same factor suggests that the cause of the difference lies in the radial quadrupole integrals used in the two calculations. There is configuration interaction between the terms of the 3d⁷ electron configuration and the 3d⁶4d configuration in our calculation and not in the single configuration calculation of Hansen *et al* (1984). With this interaction included, the quadrupole line strength involves both the 3d radial quadrupole integral and the 4d integral which is significantly larger than for the 3d.

Fivet *et al* (2016) have made calculations of forbidden transition probabilities for the twice ionised iron-peak elements from Sc to Ni, including Co, and we compare with their results in Table 10. Their calculations were made with two different methods which we label as FQB1 and FQB2. The FQB2 values were computed with AUTOSTRUCTURE as in the present work. Apart from the magnetic dipole transitions between the levels of the ground term, which agree to all tabulated figures, the FQB2 results for the electric quadrupole transitions between levels of different terms are systematically larger than the present work by 15-20% with half of them differing by the same fixed amount of 19%.

As discussed above in the comparison with the work of Hansen *et al* (1984), the systematic nature of the difference suggests that it is due to a different value for the 3d radial quadrupole integral rather than details of the wave function expansions of individual terms. The configuration expansions in the present work and in that of Fivet *et al* (2016) are very similar but differ in one key aspect. We use a somewhat contracted $\bar{4}d$ orbital to allow for the differences in the 3d orbital between the $3d^7$ and $3d^64s$ configurations, while Fivet *et al* (2016) employ a spectroscopic 4d orbital but a contracted 5s orbital which provides flexibility to the spectroscopic 4s. These two different expansions give broadly similar energy levels and fine-structure but result in differences in the quadrupole radial integrals. It is not clear that either approach is necessarily superior, so the approximately 15-20% differences are probably a realistic measure of the uncertainty in the results for the electric quadrupole line strengths. We note that the results for the electric quadrupole transition probabilities from the FQB1 calculation of Fivet *et al* (2016) agree better with their FQB2 for some transitions and better with the current work for others.

3 SCATTERING CALCULATIONS

In this work we used the Breit-Pauli R-matrix method, which is detailed in Hummer *et al* (1993); Berrington *et al* (1995) and the references therein, to perform the scattering calculations. The calculations were made using the R-matrix codes³ where the serial version of the codes were used in some stages and the parallel version in others. An R-matrix boundary radius of 11.3 au defining the inner region was applied so that the most extended orbital (4p) of our target is covered. Each one of the partial waves of the scattered electron was expanded over 12 basis functions within the R-matrix boundary, and the expansion extends to a maximum of $J = 9$.

Collision strengths were computed over two non-overlapping energy meshes: a fine mesh consisting of 20000 evenly-divided intervals which goes from zero up to the highest target threshold (about 1.2 Rydberg), and a coarse mesh consisting of 2000 evenly-divided intervals which reach 1 Rydberg above the highest target threshold. The purpose of the first mesh is to cover the main resonance region while the second mesh is intended to cover the region where all scattering channels are open, up to an incident electron energy of about 2.2 Rydberg. Our results demonstrate that these meshes have achieved these purposes. In Figure 2 we illustrate our results with the computed collision strengths between the lowest four levels of the ground $3d^7\ ^4F$ term as a function of final electron energy up to 1 Rydberg above threshold. Dense and complex resonance structure can be seen in these plots due to the multiple close lying thresholds. We also show the collision strength averaged over 0.02 Rydberg intervals.

To ensure that the computed collision strengths have converged in partial wave for all the levels for which data are

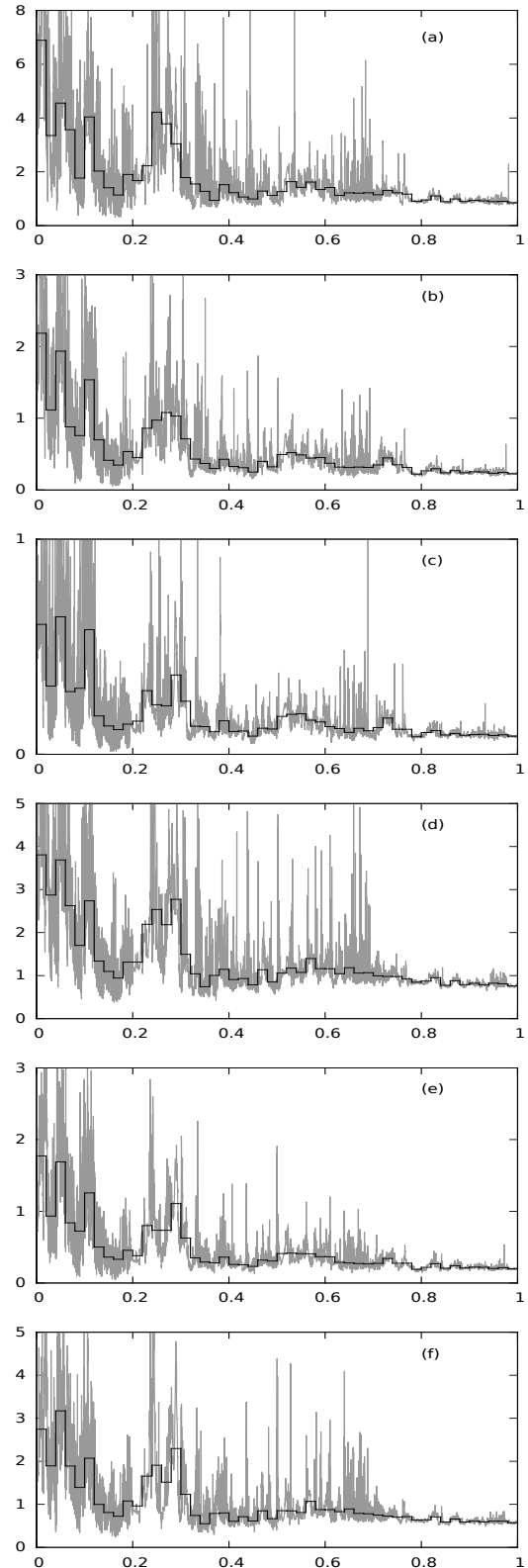


Figure 2. Collision strength (vertical axis) versus final electron energy in Rydberg (horizontal axis) for the (a) 1-2, (b) 1-3, (c) 1-4, (d) 2-3, (e) 2-4 and (f) 3-4 transitions, where the grey smooth line represents the continuous function while the black discrete line represents binned plot of the same function to show the magnitude of resonance contributions more clearly. For level indexing refer to Table 4.

³ See Badnell: R-matrix write-up on WWW. URL: amdpp.phys.strath.ac.uk/UK_RmaX/codes/.

given, the contribution of partial wave $J = 9$ was compared to the sum for all transitions and energies. This comparison showed that in almost all cases the contribution from $J = 9$ is negligible. Specifically, the largest contribution from $J = 9$ is for the transition 8-12 at about 1% and the next largest is about 0.1% of the total. However, we note that it is certain that the collision strengths from the lower levels to the levels of the 4p configuration are not converged because they are allowed transitions which have significant high partial wave contributions. We therefore do not provide collision strengths for any of these transitions.

4 RESULTS AND DISCUSSION

The thermally-averaged collision strengths between the fifteen lowest energy levels are given in Table 11 as a function of electron temperature. These values were calculated using the full energy range, as described above. In the energy region where all scattering channels are open there are some small irregular features in the collision strengths that are almost certainly non-physical and caused by the correlation orbital in the target representation. We computed thermally-averaged collision strengths for the transitions and temperature range given in Table 11 both including and excluding the contribution from the region of all channels open, and found the largest change for any transition is 0.3% at $\log_{10}T = 4.0$, 2.4% at $\log_{10}T = 4.2$ and 9.4% at $\log_{10}T = 4.4$. The values tabulated in Table 11 were computed using the full energy range.

4.1 Principal spectral lines

We compute the predicted Co^{2+} fractional level populations using the results in Tables 10 and 11 with a fifteen level model atom including electron collisional excitation and de-excitation and radiative decay. In Tables 6 and 7 we show the resulting ten strongest lines of Co III in this model. We also ensure that the three Co III mid-infrared lines at 11.88, 16.39 and 24.06 μm are in the tables even if they are not among the ten strongest. The fifteen levels are all of even parity so all these lines are [Co III] forbidden transitions. The tabulated quantity ρ is the ratio of the energy emitted per unit time in a Co III line relative to $\text{H}\beta$ for unit Co^{2+} and H^+ ion number density. Hence for a downward transition of wavelength λ_{ij} between Co^{2+} levels j and i ,

$$\rho = \frac{f_j A_{ji} \lambda_{\text{H}\beta}}{N_e \alpha_e^{\text{H}\beta} \lambda_{ij}} \quad (1)$$

where f_j is the fraction of Co^{2+} in the upper state j , A_{ji} is the Einstein A-coefficient for the transition, $\lambda_{\text{H}\beta}$ is the $\text{H}\beta$ wavelength and $\alpha_e^{\text{H}\beta}$ is the effective recombination coefficient for $\text{H}\beta$ whose value is obtained from Storey & Hummer (1995). The values of ρ are tabulated for a temperature of 10⁴ K and for two electron densities, $N_e = 10^4 \text{ cm}^{-3}$ typical of planetary nebulae (Table 6), and $N_e = 10^7 \text{ cm}^{-3}$ more typical of SN remnants in their nebular phase (Table 7). Thus, in typical PN conditions, assuming a Co abundance of 10^{-7} with respect to H^+ by number and assuming 20% of Co is in the form of Co^{2+} , the brightest visible Co III line at 5888.5 Å would have an emissivity per unit volume 5.7×10^{-4} times that of $\text{H}\beta$. In principle this would be visible

Table 6. The emissivity ratio, ρ , of the 10 strongest lines of Co III in our 15-level model atom for electron temperature $T_e = 10^4$ K and electron number density $N_e = 10^4 \text{ cm}^{-3}$ typical of PNe. We also add the 24.06 μm line to show the relative strength of all three mid-infrared lines. The powers of 10 of the ρ values are given in brackets and i and j refer to the lower and upper levels respectively as indexed in Table 4.

j	i	Transition	λ	ρ
2	1	$3d^7 \ ^4F_{7/2} - 3d^7 \ ^4F_{9/2}$	11.88 μm	5.85(+4)
8	1	$3d^7 \ ^2G_{9/2} - 3d^7 \ ^4F_{9/2}$	5888.48Å	2.83(+4)
5	1	$3d^7 \ ^4P_{5/2} - 3d^7 \ ^4F_{9/2}$	6576.31Å	2.27(+4)
3	2	$3d^7 \ ^4F_{5/2} - 3d^7 \ ^4F_{7/2}$	16.39 μm	1.26(+4)
8	2	$3d^7 \ ^2G_{9/2} - 3d^7 \ ^4F_{7/2}$	6195.45Å	8.47(+3)
6	2	$3d^7 \ ^4P_{3/2} - 3d^7 \ ^4F_{7/2}$	6853.53Å	6.93(+3)
5	2	$3d^7 \ ^4P_{5/2} - 3d^7 \ ^4F_{7/2}$	6961.53Å	5.83(+3)
13	2	$3d^7 \ ^2D_{5/2} - 3d^7 \ ^4F_{7/2}$	4499.67Å	4.07(+3)
6	3	$3d^7 \ ^4P_{3/2} - 3d^7 \ ^4F_{5/2}$	7152.69Å	3.91(+3)
12	8	$3d^7 \ ^2H_{11/2} - 3d^7 \ ^2G_{9/2}$	1.741 μm	3.82(+3)
4	3	$3d^7 \ ^4F_{3/2} - 3d^7 \ ^4F_{5/2}$	24.06 μm	1.94(+3)

Table 7. The emissivity ratio, ρ , of the 10 strongest lines plus the three mid-infrared lines of Co III with $N_e = 10^7 \text{ cm}^{-3}$ typical of SN remnants. The other details are as in Table 6.

j	i	Transition	λ	ρ
8	1	$3d^7 \ ^2G_{9/2} - 3d^7 \ ^4F_{9/2}$	5888.48Å	1.26(+4)
13	2	$3d^7 \ ^2D_{5/2} - 3d^7 \ ^4F_{7/2}$	4499.67Å	5.39(+3)
9	2	$3d^7 \ ^2G_{7/2} - 3d^7 \ ^4F_{7/2}$	5906.78Å	3.82(+3)
8	2	$3d^7 \ ^2G_{9/2} - 3d^7 \ ^4F_{7/2}$	6195.45Å	3.78(+3)
9	3	$3d^7 \ ^2G_{7/2} - 3d^7 \ ^4F_{5/2}$	6127.67Å	2.74(+3)
5	1	$3d^7 \ ^4P_{5/2} - 3d^7 \ ^4F_{9/2}$	6576.31Å	2.62(+3)
15	3	$3d^7 \ ^2D_{3/2} - 3d^7 \ ^4F_{5/2}$	4387.52Å	2.38(+3)
15	4	$3d^7 \ ^2D_{3/2} - 3d^7 \ ^4F_{3/2}$	4469.02Å	1.24(+3)
6	2	$3d^7 \ ^4P_{3/2} - 3d^7 \ ^4F_{7/2}$	6853.53Å	9.23(+2)
14	8	$3d^7 \ ^2H_{9/2} - 3d^7 \ ^2G_{9/2}$	1.548 μm	7.49(+2)
2	1	$3d^7 \ ^4F_{7/2} - 3d^7 \ ^4F_{9/2}$	11.88 μm	6.76(+2)
3	2	$3d^7 \ ^4F_{5/2} - 3d^7 \ ^4F_{7/2}$	16.39 μm	2.17(+2)
4	3	$3d^7 \ ^4F_{3/2} - 3d^7 \ ^4F_{5/2}$	24.06 μm	3.26(+1)

in deep spectra of bright PNe (e.g. Baluteau *et al* (1995)). In practice, Baluteau *et al* (1995) do not identify this line in the spectrum of NGC 7027 which may reflect depletion of gas phase Co on dust grains.

In Storey *et al* (2016) we reported collision strengths and transition probabilities for low-lying transitions in Co II and discussed the spectroscopic uses of the three mid-infrared lines at 10.52, 14.74 and 15.46 μm . There are also significant Co II visible and near-infrared lines which were not discussed by Storey *et al* (2016), so in Tables 8 and 9 we show the strongest of these. The Co II model atom also comprises the energetically lowest 15 levels and the transition probabilities and thermally-averaged collision strengths required are all from Storey *et al* (2016).

5 CONCLUSIONS

In this study, the Co III forbidden lines arising from transitions between the fifteen lowest energy levels of doubly-ionised cobalt, Co^{2+} , have been investigated. Radiative transition probabilities and collision strengths for excitation and de-excitation by electron scattering, with their thermally-averaged values based on a Maxwell-Boltzmann statistics,

Table 8. The emissivity ratio, ρ , of the 10 strongest lines of Co II with $N_e = 10^4 \text{ cm}^{-3}$ typical of PNe. We also add the 15.46 μm line discussed by Storey *et al* (2016). The other details are as in Table 6.

j	i	Transition	λ	ρ
9	1	$3d^7 4s^3 F_4 - 3d^8^3 F_4$	1.019 μm	1.17(+5)
9	4	$3d^7 4s^3 F_4 - 3d^7 4s^5 F_5$	1.547 μm	6.53(+4)
2	1	$3d^8^3 F_3 - 3d^8^3 F_4$	10.52 μm	3.81(+4)
5	4	$3d^7 4s^5 F_4 - 3d^7 4s^5 F_5$	14.74 μm	2.86(+4)
12	2	$3d^8^1 D_2 - 3d^8^3 F_3$	9342.56 \AA	1.74(+4)
9	2	$3d^7 4s^3 F_4 - 3d^8^3 F_3$	1.128 μm	1.27(+4)
9	6	$3d^7 4s^3 F_4 - 3d^7 4s^5 F_3$	1.903 μm	9.33(+3)
13	2	$3d^8^3 P_2 - 3d^8^3 F_3$	8121.13 \AA	9.04(+3)
12	3	$3d^8^1 D_2 - 3d^8^3 F_2$	9943.60 \AA	8.13(+3)
10	2	$3d^7 4s^3 F_3 - 3d^8^3 F_3$	1.025 μm	7.27(+3)
3	2	$3d^8^3 F_2 - 3d^8^3 F_3$	15.46 μm	5.00(+3)

Table 9. The emissivity ratio, ρ , of the 10 strongest lines of Co II with $N_e = 10^7 \text{ cm}^{-3}$ typical of SN remnants. We also add the 10.52, 14.74 and 15.46 μm lines discussed by Storey *et al* (2016). The other details are as in Table 6.

j	i	Transition	λ	ρ
12	2	$3d^8^1 D_2 - 3d^8^3 F_3$	9342.56 \AA	4.25(+3)
9	1	$3d^7 4s^3 F_4 - 3d^8^3 F_4$	1.019 μm	2.41(+3)
12	3	$3d^8^1 D_2 - 3d^8^3 F_2$	9943.60 \AA	1.99(+3)
13	2	$3d^8^3 P_2 - 3d^8^3 F_3$	8121.13 \AA	1.72(+3)
9	4	$3d^7 4s^3 F_4 - 3d^7 4s^5 F_5$	1.547 μm	1.35(+3)
10	2	$3d^7 4s^3 F_3 - 3d^8^3 F_3$	1.025 μm	1.07(+3)
13	1	$3d^8^3 P_2 - 3d^8^3 F_4$	7539.01 \AA	9.27(+2)
11	2	$3d^7 4s^3 F_2 - 3d^8^3 F_3$	9639.21 \AA	8.72(+2)
11	3	$3d^7 4s^3 F_2 - 3d^8^3 F_2$	1.028 μm	8.70(+2)
10	1	$3d^7 4s^3 F_3 - 3d^8^3 F_4$	9335.84 \AA	7.67(+2)
2	1	$3d^8^3 F_3 - 3d^8^3 F_4$	10.52 μm	4.46(+2)
5	4	$3d^7 4s^5 F_4 - 3d^7 4s^5 F_5$	14.74 μm	1.41(+2)
3	2	$3d^8^3 F_2 - 3d^8^3 F_3$	15.46 μm	8.48(+1)

have been computed and reported. The scattering calculations used the R-matrix method in the Breit-Pauli approximation under an intermediate coupling scheme.

The emissivities of the Co III forbidden lines were calculated with a 15-level Co^{2+} model atom and the strongest lines listed with their expected strength relative to $\text{H}\beta$ for conditions approximately representative of those in planetary nebulae and supernova remnants. For comparison and completeness we also listed the strongest forbidden lines from Co II in the same conditions based on atomic parameters calculated and presented in a previous paper (Storey *et al* 2016).

6 ACKNOWLEDGMENTS & STATEMENT

The authors would like to thank the reviewer for drawing their attention to the recent work of Fivet *et al* (2016) and suggesting the comparison. PJS acknowledges financial support from the Atomic Physics for Astrophysics Project (APAP) funded by the Science and Technology Facilities Council (STFC). The collision strength data, as a function of electron energy, for the lowest 15 levels of Co^+ and Co^{2+} can be obtained in electronic format with full precision from the Centre de Données astronomiques de Strasbourg (CDS) database.

REFERENCES

- Axelrod T.S., 1980, PhD thesis (UCRL-52994), University of California Santa Cruz
- Badnell N.R., 2011, *Comput. Phys. Commun.* 182, 1528
- Baluteau J.P., Zavagno A., Morisset C., Péquignot D., 1995, *A&A*, 303, 175
- Berrington K.A., Burke P.G., Chang J.J., Chivers A.T., Robb W.D., Taylor K.T., 1974, *Comput. Phys. Commun.*, 8, 149
- Berrington K.A., Burke P.G., Butler K., Seaton M.J., Storey P.J., Taylor K.T., Yu Yan., 1987, *J. Phys. B*, 20, 6379
- Berrington K.A., Eissner W.B., Norrington P.H., 1995, *Comput. Phys. Commun.*, 92, 290
- Bowers E.J.C., Meikle W.P.S., Geballe T.R., *et al*, 1997, *MNRAS*, 290, 663
- Childress M.J., Hillier D.J., Seitenzahl I., *et al*, 2015, *MNRAS*, 454, 3816
- Churazov E., Sunyaev R., Isern J., *et al*, 2014, *Nature*, 512, 406
- Colgate S.A., McKee C., 1969, *ApJ*, 157, 623
- Dessart L., Hillier D.J., Blondin S., Khokhlov A., 2014, *MNRAS*, 439, 3114
- Eissner W., Jones M., Nussbaumer H., 1974, *Comput. Phys. Commun.*, 8, 270
- Fang X., Liu X.-W., 2011, *MNRAS*, 415, 181
- Fivet V., Quinet P., Bautista M.A., 2016, *A&A*, 585, A121
- Hansen J.E., Raassen A.J.J., Uylings P.H.M., 1984, *ApJ*, 277, 435
- Hummer D.G., Berrington K.A., Eissner W., Pradhan A.K., Saraph H.E., Tully J.A., 1993, *A&A*, 279, 298
- Kuchner M.J., Kirshner R.P., Pinto P.A., Leibundgut B., 1994, *ApJ*, 426, L89
- Liu W., Jeffery D.J., Schultz D.R., Quinet P., Shaw J., Pindzola M.S., 1997, *ApJ*, 489, L141
- Nussbaumer H., Storey P.J., 1978, *A&A*, 64, 139
- Nussbaumer H., Storey P.J., 1988, *A&A*, 200, L25
- Pottasch S.R., Surendiranath R., 2005, *A&A*, 444, 861
- Storey P.J., Hummer D.G., 1995, *MNRAS*, 272, 41
- Storey P.J., Zeippen C.J., Sochi T., 2016, *MNRAS*, 456, 1974
- Sugar J., Corliss C., 1981, *J. Phys. Chem. Ref. Data*, 10, 1097
- Sugar J., Corliss C., 1985, *J. Phys. Chem. Ref. Data*, 14, 1
- Sunderland A.G., Noble C.J., Burke V.M., Burke P.G., 2002, *Comput. Phys. Commun.*, 145, 311
- Tankosić D., Popović L.C., Dimitrijević M.S., 2003, *A&A*, 399, 795
- Varani G.F., Meikle W.P.S., Spyromilio J., Allen D.A., 1990, *MNRAS*, 245, 570
- Wang W., Liu X.-W., 2007, *MNRAS*, 381, 669
- Zhang Y., Liu X.-W., Luo S.-G., Péquignot D., Barlow M.J., 2005, *A&A*, 442, 249

Table 10. Transition probabilities in s^{-1} among the energetically lowest 15 levels of Co^{2+} as obtained from the current work (CW), from Hansen *et al* (1984) (HRU), from Fivet *et al* (2016) using HFR (FQB1) and from Fivet *et al* (2016) using AUTOSTRUCTURE (FQB2). The transition indices i and j , which refer to the lower and upper levels respectively, are as in Table 4. Only the CW transition probabilities that are at least 1% of the total probability from a given upper level are listed. The powers of 10 by which the numbers are to be multiplied are given in brackets.

Transition		A-value				Transition		A-value			
j	i	CW	HRU	FQB1	FQB2	j	i	CW	HRU	FQB1	FQB2
2	1	2.00(-2)	2.0(-2)	2.01(-2)	2.00(-2)	11	3	2.23(-3)	2.2(-3)		
3	2	1.31(-2)	1.3(-2)	1.32(-2)	1.31(-2)	11	4	2.69(-3)	2.4(-3)		
4	3	4.63(-3)	4.7(-3)	4.65(-3)	4.63(-3)	11	7	1.77(-1)	2.0(-1)	1.98(-1)	2.01(-1)
5	1	5.55(-2)	4.8(-2)	6.59(-2)	6.65(-2)	11	10	6.42(-3)	6.4(-3)		
5	2	1.51(-2)	1.35(-2)	1.74(-2)	1.78(-2)	12	1	6.02(-4)	6.2(-4)		
5	3	3.14(-3)	2.68(-3)			12	8	3.94(-2)	4.2(-2)	4.29(-2)	4.69(-2)
6	2	3.14(-2)	2.7(-2)	3.69(-2)	3.73(-2)	13	2	7.34(-1)	7.5(-1)	7.44(-1)	8.27(-1)
6	3	1.85(-2)	1.63(-2)	2.18(-2)	2.21(-2)	13	3	7.94(-2)	8.1(-2)		
6	4	5.14(-3)	4.41(-3)			13	4	3.65(-2)	3.5(-2)		
7	3	2.30(-2)	2.0(-2)	2.71(-2)	2.73(-2)	13	5	4.74(-2)	4.7(-2)		
7	4	3.02(-2)	2.6(-2)	3.57(-2)	3.60(-2)	13	6	2.38(-2)	2.4(-2)		
7	6	2.45(-3)	2.5(-3)			13	10	1.87(-2)	1.8(-2)		
8	1	3.71(-1)	4.0(-1)	3.91(-1)	4.34(-1)	14	1	3.61(-3)	4.32(-3)		
8	2	1.17(-1)	1.2(-1)	1.22(-1)	1.36(-1)	14	2	1.90(-3)	2.24(-3)		
9	1	1.38(-2)	1.4(-2)			14	8	1.23(-1)	1.3(-1)	1.33(-1)	1.46(-1)
9	2	1.40(-1)	1.5(-1)	1.50(-1)	1.67(-1)	14	9	3.70(-2)	3.9(-2)	4.03(-2)	4.41(-2)
9	3	1.04(-1)	1.1(-1)	1.12(-1)	1.24(-1)	14	12	5.26(-3)	5.3(-3)		
9	8	7.19(-3)	7.2(-3)			15	3	6.93(-1)	7.3(-1)	7.34(-1)	8.02(-1)
10	2	5.36(-3)	5.1(-3)			15	4	3.67(-1)	3.9(-1)	3.86(-1)	4.19(-1)
10	3	6.52(-2)	6.43(-2)	6.20(-2)	8.08(-2)	15	6	1.52(-2)	1.4(-2)		
10	4	4.64(-2)	4.46(-2)	4.27(-2)	5.52(-2)	15	10	1.49(-1)	1.5(-1)	1.41(-1)	1.67(-1)
10	5	1.41(-1)	1.5(-1)	1.55(-1)	1.58(-1)	15	11	2.71(-2)	2.7(-2)		
10	6	7.26(-2)	8.0(-2)	8.04(-2)	8.08(-2)	15	13	2.43(-2)	2.5(-2)		
10	7	3.01(-2)	3.3(-2)								

Table 11: Thermally-averaged collision strengths among the 15 energetically lowest levels of Co^{2+} as a function of \log_{10} of temperature in Kelvin where i and j refer to the index of the lower and upper level respectively (see Table 4 for indexing).

i	j	$\log_{10}T$												
		2.0	2.2	2.4	2.6	2.8	3.0	3.2	3.4	3.6	3.8	4.0	4.2	4.4
1	2	4.037	4.171	4.321	4.573	5.001	5.470	5.699	5.586	5.229	4.732	4.177	3.636	3.135
1	3	1.490	1.471	1.511	1.630	1.795	1.926	1.957	1.893	1.769	1.607	1.419	1.228	1.045
1	4	0.429	0.448	0.473	0.502	0.528	0.545	0.544	0.529	0.505	0.473	0.429	0.378	0.325
1	5	1.285	1.328	1.379	1.409	1.404	1.364	1.299	1.226	1.177	1.182	1.221	1.243	1.224
1	6	0.578	0.611	0.626	0.618	0.590	0.551	0.509	0.471	0.456	0.472	0.497	0.506	0.490
1	7	0.232	0.215	0.201	0.188	0.178	0.171	0.164	0.156	0.155	0.160	0.167	0.168	0.162
1	8	0.963	0.944	0.937	0.949	0.973	0.997	1.027	1.071	1.115	1.154	1.193	1.225	1.235
1	9	0.312	0.322	0.315	0.299	0.282	0.270	0.267	0.274	0.283	0.292	0.302	0.309	0.308
1	10	0.361	0.377	0.404	0.422	0.421	0.407	0.393	0.384	0.373	0.361	0.349	0.340	0.332
1	11	0.180	0.166	0.147	0.127	0.109	0.094	0.084	0.077	0.073	0.072	0.073	0.077	0.081
1	12	4.532	3.989	3.412	2.884	2.444	2.093	1.805	1.570	1.407	1.330	1.316	1.327	1.328
1	13	0.375	0.369	0.374	0.393	0.417	0.430	0.431	0.428	0.431	0.442	0.463	0.486	0.500
1	14	0.374	0.374	0.364	0.342	0.313	0.284	0.259	0.242	0.238	0.244	0.254	0.261	0.260
1	15	0.070	0.066	0.065	0.066	0.068	0.070	0.073	0.075	0.078	0.081	0.086	0.090	0.092
2	3	3.301	3.280	3.245	3.264	3.382	3.536	3.617	3.581	3.442	3.209	2.905	2.578	2.258
2	4	0.732	0.760	0.831	0.962	1.139	1.315	1.428	1.457	1.415	1.319	1.184	1.034	0.884
2	5	1.089	1.064	1.046	1.026	0.987	0.930	0.864	0.804	0.772	0.785	0.820	0.838	0.816
2	6	0.658	0.682	0.695	0.690	0.668	0.639	0.606	0.571	0.544	0.540	0.552	0.559	0.551
2	7	0.292	0.274	0.254	0.233	0.215	0.203	0.192	0.183	0.185	0.202	0.223	0.232	0.227
2	8	0.617	0.610	0.602	0.601	0.603	0.605	0.609	0.625	0.648	0.673	0.698	0.716	0.719
2	9	0.490	0.487	0.474	0.461	0.451	0.447	0.454	0.472	0.489	0.501	0.512	0.521	0.524
2	10	0.231	0.230	0.240	0.258	0.275	0.284	0.284	0.281	0.278	0.277	0.281	0.282	0.278
2	11	0.177	0.188	0.195	0.191	0.178	0.160	0.143	0.132	0.125	0.121	0.120	0.120	0.118
2	12	1.319	1.343	1.329	1.257	1.137	0.998	0.862	0.753	0.686	0.664	0.673	0.690	0.697
2	13	0.354	0.349	0.340	0.335	0.338	0.344	0.347	0.351	0.358	0.372	0.388	0.398	0.397
2	14	0.593	0.590	0.585	0.573	0.551	0.523	0.495	0.472	0.464	0.475	0.497	0.523	0.539
2	15	0.163	0.157	0.153	0.150	0.151	0.155	0.161	0.166	0.171	0.177	0.184	0.193	0.200
3	4	1.591	1.611	1.692	1.855	2.071	2.278	2.413	2.462	2.436	2.327	2.143	1.923	1.696
3	5	1.016	0.953	0.886	0.822	0.752	0.677	0.607	0.550	0.518	0.518	0.533	0.538	0.518
3	6	0.544	0.574	0.594	0.592	0.568	0.535	0.501	0.469	0.448	0.448	0.463	0.474	0.467
3	7	0.301	0.283	0.264	0.248	0.240	0.238	0.236	0.231	0.231	0.243	0.262	0.274	0.273
3	8	0.343	0.344	0.342	0.340	0.336	0.329	0.323	0.322	0.326	0.332	0.342	0.350	0.351
3	9	0.509	0.493	0.476	0.466	0.462	0.464	0.475	0.498	0.520	0.537	0.553	0.565	0.569
3	10	0.129	0.130	0.140	0.155	0.171	0.181	0.184	0.182	0.179	0.181	0.188	0.193	0.192
3	11	0.151	0.159	0.172	0.184	0.185	0.176	0.161	0.150	0.142	0.139	0.138	0.136	0.132
3	12	0.312	0.358	0.393	0.401	0.384	0.350	0.312	0.280	0.262	0.261	0.272	0.285	0.292
3	13	0.251	0.244	0.232	0.220	0.213	0.212	0.216	0.223	0.232	0.243	0.255	0.262	0.259
3	14	0.627	0.625	0.640	0.646	0.628	0.591	0.550	0.519	0.507	0.516	0.541	0.572	0.595
3	15	0.179	0.177	0.175	0.175	0.177	0.184	0.193	0.202	0.211	0.221	0.234	0.245	0.250
4	5	0.910	0.818	0.721	0.631	0.546	0.467	0.398	0.342	0.306	0.293	0.291	0.288	0.275
4	6	0.373	0.394	0.404	0.394	0.369	0.340	0.314	0.291	0.281	0.291	0.311	0.324	0.320
4	7	0.261	0.248	0.233	0.223	0.220	0.223	0.226	0.225	0.224	0.228	0.240	0.250	0.251
4	8	0.163	0.166	0.166	0.164	0.159	0.151	0.143	0.138	0.134	0.131	0.131	0.133	0.133
4	9	0.376	0.365	0.356	0.355	0.359	0.365	0.376	0.396	0.416	0.431	0.444	0.456	0.461
4	10	0.059	0.067	0.078	0.089	0.099	0.104	0.105	0.102	0.100	0.102	0.109	0.116	0.118
4	11	0.106	0.105	0.117	0.135	0.147	0.146	0.137	0.127	0.122	0.119	0.118	0.116	0.111
4	12	0.053	0.056	0.062	0.067	0.069	0.069	0.067	0.065	0.065	0.068	0.075	0.081	0.085
4	13	0.161	0.154	0.143	0.130	0.119	0.111	0.108	0.109	0.111	0.116	0.124	0.130	0.132
4	14	0.494	0.501	0.525	0.538	0.525	0.492	0.453	0.420	0.403	0.407	0.429	0.458	0.480
4	15	0.145	0.146	0.146	0.147	0.150	0.157	0.167	0.177	0.187	0.200	0.213	0.223	0.226
5	6	1.391	1.531	1.673	1.759	1.760	1.676	1.526	1.343	1.171	1.043	0.961	0.910	0.875
5	7	0.900	0.835	0.777	0.732	0.689	0.636	0.570	0.499	0.439	0.403	0.386	0.381	0.378
5	8	0.518	0.490	0.473	0.473	0.486	0.493	0.480	0.449	0.407	0.367	0.340	0.328	0.324
5	9	0.339	0.343	0.330	0.304	0.272	0.239	0.210	0.184	0.163	0.146	0.136	0.132	0.133
5	10	0.205	0.197	0.205	0.225	0.242	0.250	0.249	0.245	0.243	0.249	0.263	0.281	0.291
5	11	0.143	0.131	0.118	0.106	0.096	0.089	0.084	0.083	0.083	0.084	0.087	0.089	0.089

Table 11: continued.

i	j	$\log_{10}T$												
		2.0	2.2	2.4	2.6	2.8	3.0	3.2	3.4	3.6	3.8	4.0	4.2	4.4
5	12	0.265	0.273	0.297	0.332	0.364	0.379	0.376	0.362	0.348	0.345	0.356	0.374	0.388
5	13	0.519	0.495	0.453	0.407	0.364	0.328	0.302	0.287	0.282	0.284	0.289	0.299	0.309
5	14	0.144	0.134	0.121	0.108	0.097	0.089	0.083	0.079	0.079	0.084	0.092	0.101	0.106
5	15	0.116	0.115	0.115	0.114	0.116	0.124	0.135	0.145	0.153	0.158	0.162	0.167	0.169
6	7	0.656	0.614	0.589	0.580	0.570	0.546	0.507	0.458	0.411	0.373	0.348	0.333	0.323
6	8	0.247	0.239	0.233	0.232	0.236	0.235	0.227	0.211	0.192	0.173	0.160	0.154	0.152
6	9	0.333	0.315	0.295	0.276	0.258	0.240	0.222	0.204	0.187	0.173	0.165	0.162	0.163
6	10	0.105	0.110	0.123	0.141	0.157	0.167	0.172	0.175	0.178	0.184	0.195	0.205	0.210
6	11	0.176	0.161	0.144	0.128	0.114	0.102	0.094	0.090	0.091	0.094	0.099	0.106	0.108
6	12	0.096	0.113	0.138	0.158	0.164	0.159	0.148	0.137	0.127	0.122	0.123	0.127	0.131
6	13	0.270	0.259	0.242	0.222	0.203	0.188	0.178	0.173	0.173	0.175	0.180	0.187	0.192
6	14	0.193	0.187	0.181	0.175	0.169	0.163	0.159	0.156	0.154	0.156	0.164	0.176	0.184
6	15	0.088	0.088	0.088	0.087	0.087	0.090	0.095	0.103	0.111	0.119	0.125	0.131	0.136
7	8	0.077	0.077	0.080	0.086	0.092	0.094	0.090	0.082	0.072	0.062	0.053	0.048	0.045
7	9	0.164	0.157	0.152	0.149	0.147	0.144	0.138	0.130	0.120	0.111	0.105	0.104	0.103
7	10	0.035	0.037	0.043	0.053	0.063	0.070	0.074	0.076	0.077	0.079	0.082	0.084	0.085
7	11	0.105	0.101	0.095	0.088	0.079	0.071	0.065	0.062	0.063	0.066	0.071	0.076	0.078
7	12	0.025	0.042	0.061	0.071	0.070	0.060	0.049	0.039	0.031	0.026	0.024	0.023	0.024
7	13	0.114	0.113	0.108	0.101	0.094	0.086	0.081	0.077	0.076	0.075	0.075	0.077	0.079
7	14	0.138	0.135	0.132	0.129	0.125	0.121	0.118	0.115	0.113	0.113	0.118	0.125	0.132
7	15	0.043	0.043	0.043	0.044	0.046	0.048	0.051	0.055	0.059	0.063	0.067	0.071	0.075
8	9	1.248	1.372	1.481	1.552	1.573	1.557	1.531	1.501	1.448	1.388	1.369	1.406	1.445
8	10	0.419	0.446	0.483	0.516	0.543	0.570	0.594	0.606	0.601	0.581	0.561	0.550	0.544
8	11	0.411	0.384	0.358	0.340	0.332	0.324	0.316	0.306	0.292	0.273	0.254	0.242	0.235
8	12	1.282	1.265	1.281	1.321	1.362	1.385	1.383	1.380	1.434	1.596	1.839	2.063	2.164
8	13	0.735	0.717	0.692	0.664	0.643	0.628	0.615	0.607	0.607	0.629	0.689	0.775	0.841
8	14	0.956	0.989	1.015	1.033	1.039	1.025	1.000	0.978	0.990	1.058	1.160	1.247	1.278
8	15	0.358	0.372	0.386	0.391	0.387	0.376	0.363	0.349	0.339	0.341	0.362	0.395	0.418
9	10	0.493	0.429	0.384	0.367	0.376	0.401	0.427	0.446	0.453	0.445	0.437	0.437	0.440
9	11	0.411	0.390	0.386	0.402	0.417	0.414	0.395	0.372	0.346	0.318	0.297	0.288	0.286
9	12	0.426	0.516	0.639	0.763	0.846	0.874	0.862	0.838	0.830	0.856	0.909	0.962	0.988
9	13	0.422	0.410	0.402	0.396	0.395	0.398	0.405	0.415	0.428	0.450	0.490	0.539	0.574
9	14	0.990	0.967	0.940	0.909	0.878	0.856	0.847	0.856	0.915	1.055	1.248	1.413	1.482
9	15	0.293	0.315	0.342	0.364	0.376	0.381	0.382	0.382	0.383	0.392	0.420	0.464	0.498
10	11	0.357	0.338	0.334	0.349	0.371	0.387	0.403	0.427	0.446	0.451	0.450	0.449	0.440
10	12	0.158	0.174	0.192	0.199	0.190	0.172	0.154	0.143	0.144	0.156	0.173	0.186	0.189
10	13	0.587	0.573	0.558	0.547	0.546	0.557	0.580	0.609	0.635	0.660	0.695	0.731	0.747
10	14	0.099	0.098	0.097	0.095	0.095	0.098	0.102	0.106	0.115	0.129	0.144	0.154	0.156
10	15	0.423	0.454	0.495	0.534	0.558	0.571	0.578	0.575	0.562	0.549	0.542	0.540	0.530
11	12	0.053	0.064	0.075	0.080	0.076	0.068	0.059	0.052	0.050	0.054	0.058	0.060	0.058
11	13	0.319	0.296	0.275	0.259	0.255	0.265	0.284	0.302	0.313	0.321	0.332	0.344	0.350
11	14	0.042	0.041	0.040	0.040	0.042	0.046	0.050	0.055	0.061	0.068	0.076	0.083	0.087
11	15	0.178	0.198	0.227	0.258	0.285	0.304	0.313	0.310	0.297	0.283	0.276	0.274	0.268
12	13	0.343	0.332	0.316	0.299	0.286	0.283	0.292	0.310	0.336	0.368	0.400	0.425	0.434
12	14	2.767	2.722	2.622	2.476	2.301	2.119	1.958	1.841	1.805	1.880	2.050	2.241	2.361
12	15	0.073	0.072	0.073	0.079	0.088	0.098	0.106	0.114	0.130	0.151	0.169	0.179	0.178
13	14	0.164	0.168	0.171	0.171	0.171	0.171	0.174	0.182	0.197	0.220	0.247	0.269	0.277
13	15	0.295	0.302	0.314	0.328	0.346	0.378	0.427	0.481	0.526	0.564	0.610	0.659	0.688
14	15	0.160	0.162	0.170	0.185	0.200	0.212	0.222	0.232	0.246	0.261	0.277	0.293	0.301